Research Square

Preprints are preliminary reports that have not undergone peer review.
They should not be considered conclusive, used to inform clinical practice,
or referenced by the media as validated information.

Modeling Radiative Magnetohydrodynamic Mixed Convection in Second-Grade Viscoelastic Flow over a Continuously Stretching Cylinder

Abdullah Muhammad
Islamia College University
Dr. Azhar Ali
azhar.ee@suit.edu.pk

Sarhad University of Science and Information Technology
Aftab Alam
Islamia College University
Ibrar Hussian
Sarhad University of Science and Information Technology

Research Article

Keywords: Viscoelastic second grade fluid, Stretching cylinder, Magnetohydrodynamic, Radiation, Mixed Convection

Posted Date: September 30th, 2026

DOI: https://doi.org/10.21203/rs.3.rs-10809891/v1

License: This work is licensed under a Creative Commons Attribution 4.0 International License.
Read Full License

Additional Declarations: No competing interests reported.

Modeling Radiative Magnetohydrodynamic Mixed Convection in Second-Grade Viscoelastic Flow over a Continuously Stretching Cylinder

Muhammad Abdullah [a], Azhar Ali [b*], Aftab Alam [a], Ibrar Hussain [a]

[a]Department of Mathematics, Faculty of Technologies and Engineering Sciences, Islamia College Peshawar 25120, Jamrod Road, University Campus, Peshawar, Khyber Pakhtunkhwa, Pakistan

[b]Department of Mathematics, Faculty of Sciences, Computer Science and IT, Sarhad University of Science and Information Technology, Peshawar, Pakistan

Abstract

Motivated by its significance in industrial operations such as polymer extrusion, chemical manufacturing, and thermal processing, this study investigates the radiative magnetohydrodynamic (MHD) mixed convection flow of a second-grade viscoelastic fluid over a continuously stretching cylinder. Unlike conventional analyses based on flat stretching sheets, the present configuration incorporates curvature effects, thereby offering a more realistic representation of cylindrical extrusion and coating processes. The governing boundary layer equations are transformed into a coupled system of nonlinear ordinary differential equations using appropriate similarity transformations. A key mathematical challenge arises because the obtained fourth-order nonlinear momentum ODE is subject to only three boundary conditions. The mismatch between the high order of the coupled ODEs and the limited boundary conditions presents a distinct uniqueness challenge. We overcome this by imposing an additional constraint derived from mass conservation that is introduced to uniquely determine the system. The alignment of multiple obtained solutions demonstrates robustness. Crucially, instead of traditional 2D curves, the simultaneous impacts of the governing parameters are mapped using 3D surface topologies. This multi-dimensional approach successfully captures the non-linear coupling effects on the skin friction coefficient, Nusselt number, and Sherwood number, revealing critical parameter thresholds that remain obscured in conventional one-dimensional plots. Benchmarking with previously published results, further validates the robustness, accuracy, and physical reliability of the model. The findings suggest strong potential of practical significance and offer experimental investigations and engineering applications in advanced thermal management systems, including MHD generators, nuclear and solar thermal energy systems, metallurgical processing, polymer extrusion, electronic cooling modules, and high-performance heat exchangers.

Keywords: Viscoelastic second grade fluid; Stretching cylinder; Magnetohydrodynamic; Radiation; Mixed Convection.

*The correspondence author is Azhar Ali.
The correspondence author Email:azhar.ee@suit.edu.pk

Introduction

It is well established by now that the manufacture of stretchable plastics, papers, and food products revolves around non-Newtonian fluid processes involving stretched flow dynamics. These processes are significantly enhanced by the transfer of heat, water, and other mass materials. The science dealing with the properties of non-Newtonian fluid flow across impermeable stretching sheet regarding heat and mass transfer is being pursued by numerous researchers in science, engineering, and industry. Quite a number of fluids also disobey Newton's appearance of viscosity, such as paints, blood under minimal shear rates, lubricants, shampoo, ketchup, and personal hygiene items. Collectively, these fluids are termed non-Newtonian fluids. Flows of non-Newtonian fluid play an essential role in polymer processing, bubble column activities, fermentation, composite processing, boiling, and absorption of plastic foam and bubbles. Many agents are responsible for fluid motion between walls, and some of these generators are highly dynamic and powerful. The role of heat transfer is crucial to these processes. Many contemporary researchers are concerned with the investigation of properties of heat transference in non-Newtonian fluid flow across a stretching surface. Moreover, the mixed convection of MHD flow is also of enormous significance in many industrial processes such as polymer (plastic, rubber, and fiber, etc.) manufacturing and in heat exchangers.
In the last few years, classical works inspecting the causes of heat and mass transfer of fluids to stretching surface have been published. A more thorough explanation of flow of power-law fluid over a stretching sheet in non-Newtonian boundary layers was given by Andersson and Kumaran (2006). Vajravelu *et al.* (2011) investigated mass transfer and two dimensional steady flow of non-Newtonian power-law fluid caused by a stationary flat plate. Patil *et al.* (2012) investigated the effect of a nonlinear extension of a vertically upward cylinder on an unstable mixed convection boundary layer with surface thermal diffusion and mass transfer. Lok *et al.* (2012) analyzed the flow of steady mixed convection fluid around an axisymmetric stagnation point on vertical cylinders that are either stretching or shrinking. Das (2012) studied heat generation by an enlarging surface with slip effects and mixed convection stagnation point flow. Liao (2012) studied the flow and heat generation of a second-grade fluid about a horizontal cylinder under boundary layer assumptions. Nadeem *et al.* (2012) investigated how temperature-dependent thermal conduction affected heat transfer and axisymmetric magnetohydrodynamic flow due to a non-isothermal overextended cylinder while considering internal heat generation/absorption. Vajravelu *et al.* (2012) studied heat transfer by convective-radiative for an inclined flat plate embedded in a porous medium. Moradi *et al.* (2013) studied radiative effect on three-dimensional MHD flow of Eyring-Powell fluid. Hayat *et al.* (2013) investigated the impact of Newtonian heating on the MHD three-dimensional flow past a stretching surface. Ramzan *et al.* (2013) examined the phenomenon of steady convective boundary layer flow in a Jeffrey fluid model over a vertical flat plate that is either stretching or shrinking. Turkyilmazoglu and Pop (2013) considered the three dimensional boundary layer flow of a Maxwell fluid past a bi-directionally stretched sheet subject to specified temperature and heat flux at the sheet surface. Shehzad *et al.* (2013) investigated the effects of heat generation on the axisymmetric flow of a third-grade incompressible fluid between stretching surfaces. Hayat *et al.* (2013) investigated heat generation and unsteady flow of a micropolar fluid along a vertical extending sheet when a buoyancy force was added. Abd El-Aziz and Hayat (2013) examined the flow of boundary layer viscoelastic fluid using the Casson fluid model with a constant temperature on the stretching surface. Mukhopadhyay *et al.* (2013) proposed a steady MHD mixed convection control system for stretched sheets with Soret and Dufour effects. Turkyilmazoglu (2013) considered the effects of variable thermal conductivity, radiation and buoyancy on an unsteady flow with heat transfer over a vertical porous stretching surface. Vajravelu *et al.* (2013) deliberated 2-D forced convection in concentric porous cylinders filled with a viscous incompressible fluid, where mass

transfer and periodic pressure occur across the porous borders. Rashidi *et al.* (2014) discussed the transfer of melting heat in two-dimensional Maxwell fluid stagnation-point flow in the direction of a stretching surface. Mukhopadhyay and Mandal (2014) studied the conjugate heat transfer and Ohmic mixed convection in an incompressible second-grade Maxwell fluid for the first time. Hsiao's work, reported in reference (2014), focused on entropy generation related to a Jeffrey fluid's steady two-dimensional laminar flow across a sheet that is stretching linearly. Dalir (2014) studied the mixed convection flow of a second grade fluid due to an impermeable enlarging cylinder with varying surface temperature and variable thermal conductivity. Hayat *et al.* (2015) scrutinized the impact of coupled mixed convection and inconstant thermal conductivity on the flow of a viscoelastic fluid caused by an impermeable stretched cylinder. Shah et al. (2022) investigated UCM (upper-convected Maxwell) nanofluid slip flow with the effects of magnetization induced by an inclined porous stretching sheet. Raj *et al.* (2024) examined the magnetohydrodynamics (MHD), radiation, and heat generation effects on the flow of Maxwell fluid by an enlarging cylinder, identifying the often-overlooked flow and heat behavior. Zafar *et al.* (2024) examined the novel application of hybrid nanofluids in the two-dimensional magnetohydrodynamic boundary-layer flow over a stretching sheet embedded in a porous material. Jakhar *et al.* (2024) studied uniquely incorporate the Hall current, induced by the radial magnetic field, along with chemical reactions, convective boundary conditions, and variable thermal conductivity, offering a comprehensive analysis of their combined effects. Olkha *et al.* (2025) scrutinized the slip flow of a temperature-dependent, non-Newtonian second-grade fluid over a non-linear radially extending face in a porous medium, accounting for thermal radiation, viscous dissipation, and non-linear heat generation effects.

Novelty of the problem

The enormous amount of literature, as cited above, on viscoelastic fluid dynamics has contributed immensely to the understanding of boundary layer flows, heat and mass generation on stretched sheets, the impact of emission, and magnetohydrodynamics flows in different geometries. In particular, analyzing boundary layer flows in advanced biomedicine and astrophysics demonstrates the interdisciplinary applications of fluid dynamics; however, there is one major research gap that needs to be addressed, which has been ignored by all the classical studies mentioned above and that none of them have focused on the combined influence of MHD, radiation, heat and mass generation on viscoelastic second grade fluids over permeable stretching cylindrical surfaces. This study will address this research gap and explore these combined influences on viscoelastic second grade fluid flows over impermeable stretching cylinders. Our findings are highlighted in conjunction with the existing literature to validate the precision of conclusions and the reliability of our approach. Besides, we focus on the effects of involved parameters on cylindrical geometries, broadening the scope of the study and allowing us to correlate how these parameters influence flow dynamics in different contexts.

The complete description of the problem and geometrical view are depicted in Figures 1 & 2, respectively.

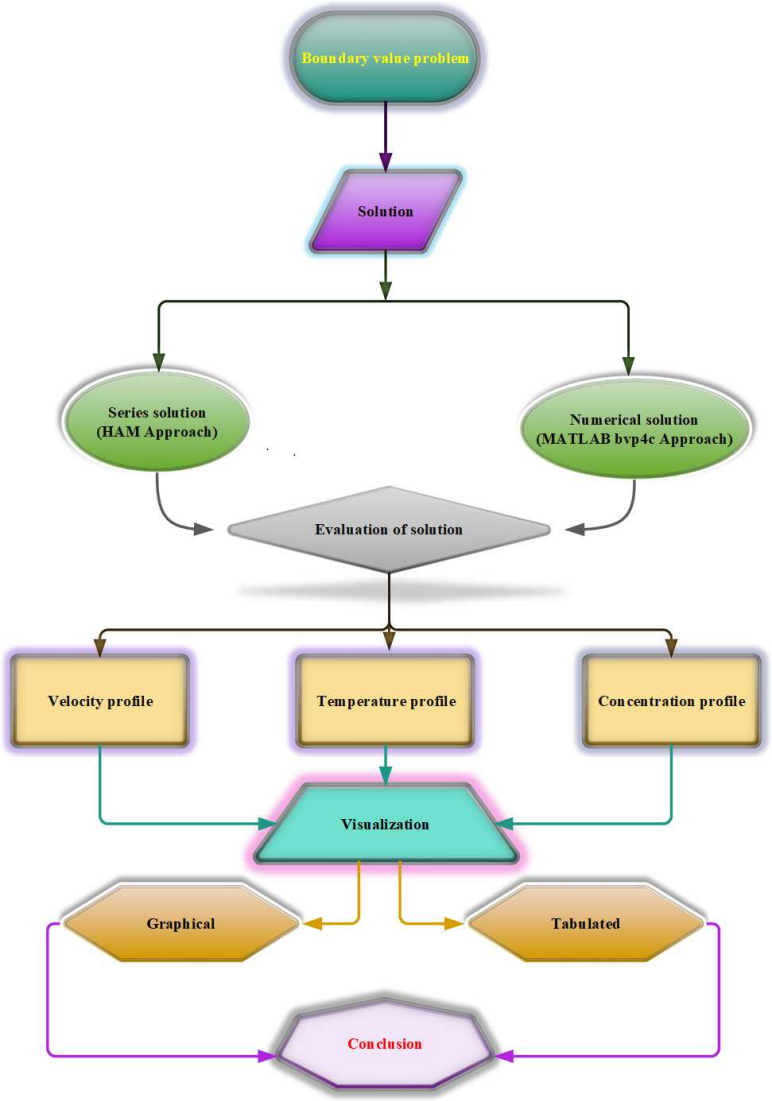


Figure 1: Flow chart of the description of the problem.

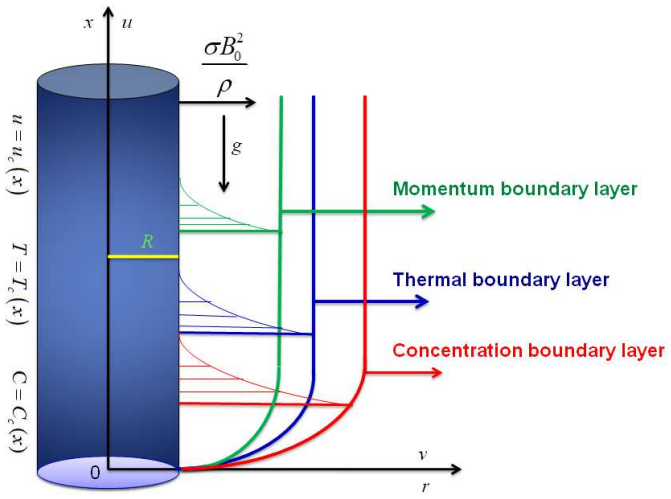


Figure 2: Schematic diagram of the problem.

Mathematical Formulation

We analyzes the steady flow of a second grade fluid in two dimensions that are incompressible and laminar due to the mixed convection along a stretching cylinder. In this analysis, the Boussinesq approximation is used for calculating the buoyancy force. The stretching velocity is created using equal forces in opposite directions on the cylinder but maintaining its origin constant. The temperature of the cylinder wall $T_c(x)$ is greater than the ambient fluid temperature T_∞. The cylinder concentration $C_c(x)$ is prescribed at the wall of the plate, while C_∞ represents the constant concentration of the species in the ambient region. Coordinate system of the cylinder takes in such a way that $x - axis$ is parallel to the axis of the cylinder and $r - axis$ is normal to it. Heat and mass transfer is analyzed by considering the variation of thermal conductivity. Furthermore, it is considered that thermal conductivity varies linearly with temperature. Effect of thermal buoyancy force is also considered. Flow due to increasing $x - axis$ and stretching cylinder is in the same direction because both stretching and thermal buoyancy forces support each other in flow field. The following equations can govern the present flow consideration:

Equation of continuity

$$\nabla.V = 0 \tag{1}$$

Equation of motion

$$\rho\frac{dV}{dt} = \nabla.\tau + \rho b \tag{2}$$

Energy equation

$$\begin{aligned}\frac{dT}{dt} = &\frac{1}{(\rho C_p)r}\frac{\partial}{\partial r}\left[K(T)r\frac{\partial T}{\partial r}\right] \\ &+ \frac{16\sigma T_\infty^3}{3(\rho C_p)k}\frac{\partial^2 T}{\partial r^2} + Q_b(T - T_\infty)\end{aligned} \tag{3}$$

Concentration equation

$$\frac{dT}{dt} = D_B[\frac{\partial^2 C}{\partial r^2} + \frac{1}{r}\frac{\partial C}{\partial r}] \tag{4}$$

Where $\frac{dv}{dt}$ represents the material derivative and the τ is the Cauchy stress tensor for second grade fluid is

$$\tau = -pI + \mu A_1 + \alpha_1 A_2 + \alpha_2 A_1^2 \tag{5}$$

The first and second Rivlin-Ericksen tensors denoted by A_1 and A_2 are defined as below

$$A_1 = grad\ V + (grad\ V)^{T^*} \tag{6}$$

Where T^* represent transpose

$$A_2 = \frac{dA_1}{dt} + A_1(grad\ V) + (grad\ V)^{T^*}A_1 \tag{7}$$

In cylindrical coordinates we have

$$grad\ V = \begin{pmatrix} \frac{\partial V_r}{\partial r} & \frac{1}{r}\frac{\partial V_r}{\partial \theta} - \frac{V_\theta}{r} & \frac{\partial V_r}{\partial x} \\ \frac{\partial V_\theta}{\partial r} & \frac{1}{r}\frac{\partial V_\theta}{\partial \theta} + \frac{V_r}{r} & \frac{\partial V_\theta}{\partial x} \\ \frac{\partial V_x}{\partial r} & \frac{1}{r}\frac{\partial V_x}{\partial \theta} & \frac{\partial V_x}{\partial x} \end{pmatrix},$$

$$\nabla.\tau = \begin{pmatrix} \frac{\partial \tau_{rr}}{\partial r} + \frac{\tau_{rr}}{r} + \frac{1}{r}\frac{\partial \tau_{\theta r}}{\partial \theta} + \frac{\partial \tau_{xr}}{x} - \frac{\tau_{\theta\theta}}{r} \\ \frac{\partial \tau_{r\theta}}{\partial r} + \frac{\tau_{r\theta}}{r} + \frac{1}{r}\frac{\partial \tau_{\theta\theta}}{\partial \theta} + \frac{\partial \tau_{x\theta}}{x} + \frac{\tau_{\theta r}}{r} \\ \frac{\partial \tau_{rx}}{\partial r} + \frac{\tau_{rx}}{r} + \frac{1}{r}\frac{\partial \tau_{\theta x}}{\partial \theta} + \frac{\partial \tau_{xx}}{x} \end{pmatrix} \tag{8}$$

Where α_1 and α_2 are the material constants. For the consistency of model with thermodynamics it is necessary that

$$\alpha_1 \geq 0,\ \mu \geq 0\ and\ \alpha_1 + \alpha_2 = 0 \tag{9}$$

Using the velocity field

$$V = [v(r,x), 0, u(r,x)] \tag{10}$$

When the governing equations (Continuity, Momentum, Energy and Concentration Equations) are simplified using boundary layer assumptions (i.e. v = O(δ), r = O(δ), u = O(1) and x = O(1)), they take the following

$$\frac{\partial (ru)}{\partial x} + \frac{\partial (rv)}{\partial r} = 0 \tag{11}$$

$$\begin{aligned} v\frac{\partial u}{\partial r} + u\frac{\partial u}{\partial x} = v\left(\frac{\partial^2 u}{\partial r^2} + \frac{1}{r}\frac{\partial u}{\partial r}\right) + \frac{\alpha_1}{\rho}\Bigg[v\frac{\partial^3 u}{\partial r^3} + u\frac{\partial^3 u}{\partial x \partial r^2} \\ - \frac{\partial^2 v}{\partial r^2}\frac{\partial u}{\partial r} + \frac{\partial u}{\partial x}\frac{\partial^2 u}{\partial r^2} + \frac{1}{r}\Big(v\frac{\partial^2 u}{\partial r^2} + u\frac{\partial^2 u}{\partial x \partial r} \\ - \frac{\partial v}{\partial r}\frac{\partial u}{\partial r} + \frac{\partial u}{\partial x}\frac{\partial u}{\partial r}\Big)\Bigg] + g\beta_T(T - T_\infty) \\ - \frac{\sigma B_0^2}{\rho}\left(v\frac{\partial u}{\partial r} + u\right) - \frac{v}{k}u \end{aligned} \tag{12}$$

$$\begin{aligned} v\frac{\partial T}{\partial r} + u\frac{\partial T}{\partial x} = \frac{1}{\rho C_p r}\frac{\partial}{\partial r}\left(K(T) r \frac{\partial T}{\partial r}\right) \\ + \frac{16\sigma T_\infty^3}{3(\rho C_P)k}\frac{\partial^2 T}{\partial r^2} + Q_b(T - T_\infty) \end{aligned} \tag{13}$$

$$v\frac{\partial C}{\partial r} + u\frac{\partial C}{\partial x} = D_B\left(\ \frac{\partial^2 C}{\partial r^2} + \frac{1}{r}\frac{\partial C}{\partial r}\ \right) \tag{14}$$

The relevant boundary conditions are mentioned below:

$$u(x,R) = u_c(x) = \tfrac{u_0 x}{l},\ v(x,R) = 0,\ T(x,R) = T_c(x) = T_\infty + \left(\ \tfrac{x}{l}\ \right)^n \Delta T,$$

$$C(x,r) = C_c(x)$$

$$u(x,r) \to 0,\ T(x,r) \to T_\infty,\ C(x,r) \to C_\infty\ as\ r \to \infty \tag{15}$$

In the above expressions u and v, ν, ρ, C_p, $u_c(x)$, u_0, l, n, σ, k, Q_b, and D_B are the velocity components in the x and r directions, kinematic viscosity, density, specific heat at constant pressure, stretching velocity of the cylinder, reference velocity, characteristics length, surface temperature exponent, Stefan-Boltzmann constant, mean absorption coefficient, dimensional heat generation, and mass diffusion, respectively. Furthermore, $T_c(x) - T_\infty = \left(\frac{x}{l}\right)^n \Delta T$ denotes characteristics temperature, T and T_∞ are the fluid and ambient temperatures respectively, $C - C_\infty = \Delta C$ represents characteristics concentration, C and C_∞ are the fluid and ambient concentrations respectively, B_0 signifies magnetic parameter, β_T shows coefficient of volumetric thermal expansion. The thermal conductivity $K(T)$ is given by

$$K(T) = K_\infty(1 + \epsilon\theta) \tag{16}$$

Where K_∞ denotes thermal conductivity of the ambient fluid, θ shows dimensionless temperature and ϵ represents a scalar parameter which shows the influence of temperature on variable thermal conductivity.
Using the transformation

$$\eta = \sqrt{\frac{u_0}{vl}}\frac{(r^2 - R^2)}{2R},\ u = \frac{u_0 x}{l}f'(\eta),\ v = -\frac{R}{r}\sqrt{\frac{u_0 v}{l}}f(\eta),$$
$$\theta(\eta) = \frac{T - T_\infty}{T_c - T_\infty},\ \phi(\eta) = \frac{C - C_\infty}{C_c - C_\infty} \tag{17}$$

Equation (11) is identically satisfied and Eqs. (12-14) are reduced as follows.

$$\begin{aligned}&(1 + 2\gamma\eta)f''' + 2\gamma f'' + ff'' + \beta_p M_p ff'' - (f')^2\\ &+ 4\gamma\beta(f'f'' - ff''') + \beta(1 + 2\gamma\eta)(2f'f''' + (f'')^2\\ &- ff'''') - M_p f' - \phi_p f' + \lambda\theta = 0\end{aligned} \tag{18}$$

$$\begin{aligned}&(1 + 2\gamma\eta)(1 + \epsilon\theta + R_p)\theta'' + 2\gamma(1 + \epsilon\theta + \tfrac{1}{2}R_p)\theta'\\ &+ \epsilon(1 + 2\gamma\eta)\theta'^2 + Pr(f\theta' - nf'\theta + Q_p\theta) = 0\end{aligned} \tag{19}$$

$$(1 + 2\gamma\eta)\phi'' + 2\gamma\phi' + S_c f\phi' = 0 \tag{20}$$

While boundary conditions reduce to the forms

$$\begin{aligned}&f(0) = 0,\quad f'(0) = 1,\quad \theta(0) = 1,\quad \phi(0) = 1\\ &f'(\eta) \to 0,\quad \theta(\eta) \to 0,\quad \phi(\eta) \to 0\ \ as\ \ \eta \to \infty\end{aligned} \tag{21}$$

Where γ, λ, Pr, R_p, S_c, M_p, ϕ_p, β_p, and β are the curvature parameter, mixed convection parameter, Prandtl number, radiation parameter, ratio of momentum diffusivity, ratio of magnetic force to inertial force in MHD, influence of a permeable medium on the flow, Maxwell fluid which personifies the viscoelastic behavior of the fluid, and viscoelastic parameter, respectively. These parameters are expressed as follows:

$$\lambda = \frac{Gr_x}{Re_x^2} = \frac{g\beta_T l^2(T_c - T_\infty)}{u_0^2 x},$$
$$Gr_x = \frac{g\beta_T(T_c - T_\infty)x^3}{\nu^2},\ M_p = \frac{\sigma B_0^2 l}{\rho u_0},$$
$$\phi_p = \frac{\nu l}{k u_0},\ \beta_p = \frac{u_0}{l},$$
$$\gamma = \sqrt{\frac{\nu l}{u_0 R^2}},\ \beta = \frac{\alpha_1 u_0}{\rho \nu l},\ Pr = \frac{\mu c_p}{K_\infty}.$$
$$S_c = \frac{v}{D_B},\ Q_p = \frac{l Q_b}{u_0},\ R_p = \frac{16\sigma T_\infty^3}{3kk_\infty} \tag{22}$$

Where Gr_x represent the local Grashof number (which is the ratio of buoyancy to viscous forces).
Skin fraction coefficient, Nusselt number and Sherwood number are defined as follows:

$$C_f = \frac{2\tau_c}{\rho u_c^2}, Nu_x = \frac{xq_c}{K(T_c - T_\infty)}, Sh_x = \frac{xj_x}{D_B(C_c - C_\infty)}. \tag{23}$$

Where wall shear stress (τ_c), heat flux (q_c) and mass flux (j_c) are

$$\tau_c = \left(\mu\frac{\partial u}{\partial r} + \alpha_1(v\frac{\partial^2 u}{\partial r^2} + u\frac{\partial^2 u}{\partial x \partial r} + \frac{\partial u}{\partial r}\frac{\partial u}{\partial x} - \frac{\partial v}{\partial r}\frac{\partial u}{\partial r}) \right)_{r=R},$$
$$q_c = -k\left(\frac{\partial T}{\partial r}) \right)_{r=R}, j_x = -D_B\left(\frac{\partial C}{\partial r}) \right)_{r=R} \tag{24}$$

Non-dimensional skin fraction coefficient, Nusselt number and Sherwood number can be expressed as

$$\frac{1}{2}C_f\sqrt{Re_x} = (1+3\beta)f''(0), \frac{Nu}{\sqrt{Re_x}} = -\theta'(0), \quad \frac{Sh}{\sqrt{Re_x}} = -\phi'(0) \tag{25}$$

In which $Re_x = \frac{u_c(x)x}{v} = \frac{u_0 x^2}{vl}$ is the local Reynolds number (which is the ratio of inertial to viscous forces).

Solution of the Problem

The system of ODEs (18–21) is solved by two complementary approaches: the Homotopy Analysis Method, which provides analytical insight through series solutions, and MATLAB's bvp4c solver, which yields precise numerical results. Employing both methods ensures accuracy and reliability by allowing cross-validation of the analytical and numerical findings. The essential features of these methods are outlined below.

Analytical Schemes

Homotopy Analysis Method comes from the basic principle of Topology called Homotopy. The two functions are called homotopic when one function can be deformed continuously to another function. Let f_1 and f_2 be two continuous functions that map from topological space X to Y then f_1 is homotopic to f_2 when there exists a continuous function F

$$F : X \times [0,1] \to Y \tag{26}$$

Such that for each $x \in X$

$$F(x,0) = f_1(x),\ F(x,1) = f_2(x) \tag{27}$$

In this case, the mapping F is said to be homotopic from f_1 to f_2. The homotopy technique does not rely on any small or large physical parameters. It is a continuous transformation or perturbation of an equation or function. There are several benefits to this method compared to other methods. These include:
(i) Independence from small/large parameters.
(ii) Ensures convergence of series solutions.
(iii) Provides great flexibility to choose the base function and linear operator.
Such flexibility helps us in solving highly nonlinear equations. It is important to note that the linear portion of the differential equation is chosen as the linear operator for the homotopy analysis method. But in the semi-infinite domain case, it is preferred in such a way that the solution takes the form of an exponential function for fast convergence analysis. Homotopy analysis method requires initial guesses $(f_0,\ \theta_0,\ \phi_0)$ and linear operators $(L_f,\ L_\theta,\ L_\phi)$ in the forms:

$$f_0(\eta) = 1 - exp(-\eta),\ \theta_0(\eta) = exp(-\eta),\ \phi_0(\eta) = exp(-\eta) \tag{28}$$

Convergence Analysis

To obtain the series solution of modeled problem in Eqs.(18-21) using HAM. In this subsection, the convergence analysis is demonstrated. The convergence and approximation rate of the constructed series solutions rely depend on the auxiliary parameters $h_f,\ h_\theta\ and\ h_\phi$. Convergence of these must be ensured. Thus, we have plotted the $h-curves$ in the Figures: $3-5$. From these graphs we observed that allowable values of $h_f,\ h_\theta\ and\ h_\phi$ are $-1.4 \leq h_f \leq 0.1,\ -0.8 \leq h_\theta \leq 0.15$ and $-2.8 \leq h_\phi \leq -0.4$ for order of approximation $12^{th}\ and\ 7^{th}$ respectively when $\lambda = 0.3, \epsilon = 0.2, \gamma = 0.1, Pr = 1, \beta = 0.2,$
$n = 2, \beta_p = 0.3, M_p = 0.1, \phi_p = 0.3, R_p = 1.3, S_c = 0.4,$ and $Q_p = 0.4$.

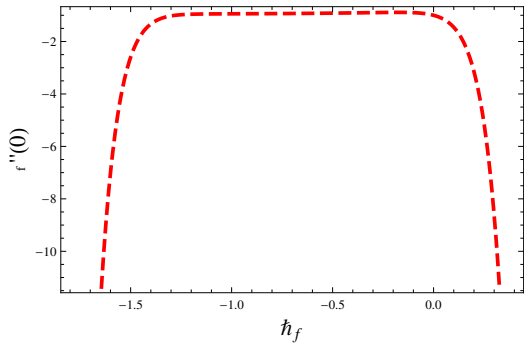


Figure 3: $h-curve$ for velocity profile.

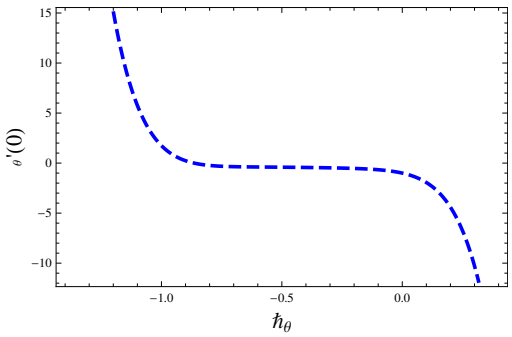


Figure 4: $h-curve$ for temperature profile.

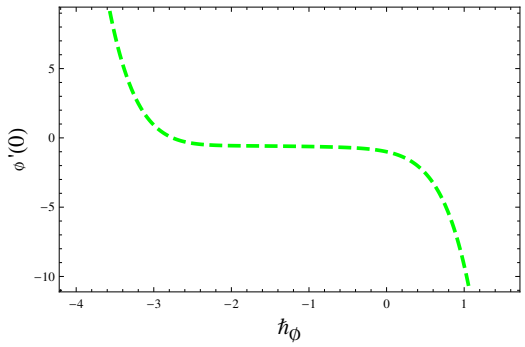


Figure 5: $h-curve$ for concentration profile.

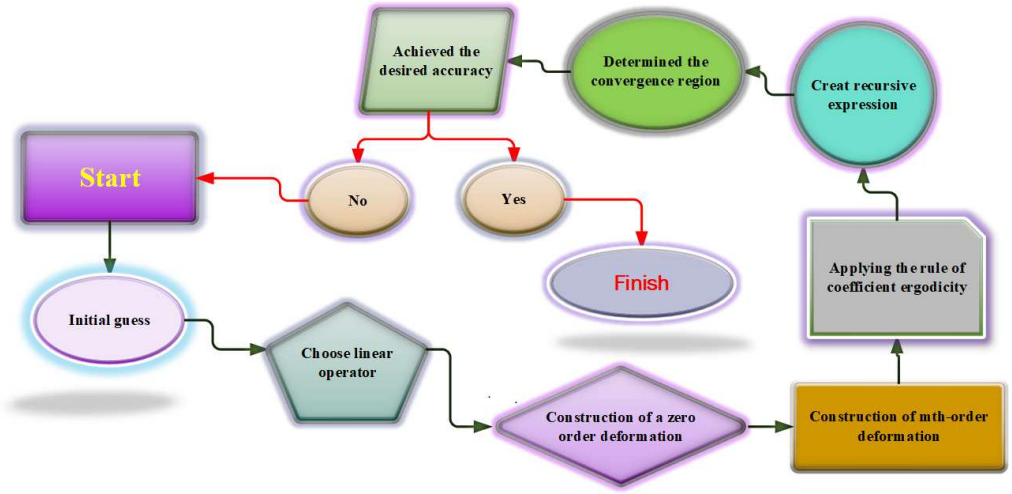


Figure 6: Flow chart of the HAM approach.

Numerical schemes

The bvp4c approach is employed to obtain the computational results for the highly nonlinear ODE's by first transforming them into a system of first-order initial value problems. This transformation is facilitated through the shooting method, which converts boundary value problems into equivalent initial value problems. Accordingly, Eqs. (18–20) are reformulated into IVPs using the following transformation process;

$y_1 = f \qquad y_5 = \theta$

$y_2 = f' \qquad y_6 = \theta'$

$y_3 = f'' \qquad y_7 = \phi$

$y_4 = f''' \qquad y_8 = \phi'$

$f4 = f''''$

The subjected boundary conditions in Eq.(21) becomes

$y_1(0) = 0, \quad y_2(0) = 1, \quad y_5(0) = 1, \quad y_7(0) = 1,$

$y_2(\infty) = 0, \quad y_5(\infty) = 0, \quad y_7(\infty) = 0, \quad y_3(\infty) = 0.$

The obtained fourth-order highly non linear momentum ODE which subject to the three boundary conditions, so an additional boundary condition $f''(\infty) = 0$ representing reasonable decay at infinity, is introduced following the approach of Sadeghy and Sharifi [30]. In the bvp4c algorithm, the number of conditions specified must match the order of the system, ensuring consistency between indices and boundary conditions.

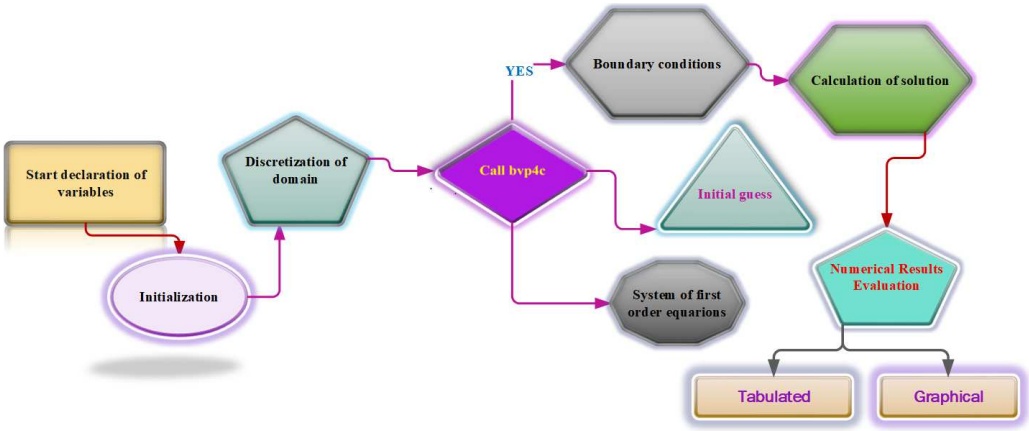


Figure 7: Flow chart of bvp4c approach.

Results and Discussion

Interpretation of the results for the series and numerical solutions regarding the effect of different physical parameters on the velocity, temperature, and concentration distributions is provided in this section. A comparative assessment is conducted between the current model and the classical formulation, as well as between the two adopted solution methods, to establish the accuracy and validity of the results. Furthermore, both tabulated and graphical analyses of the velocity, temperature, and concentration fields are provided to illustrate the effects of the governing parameters, as detailed in the subsequent subsection.

Velocity profiles

The impact of various parameters on the flow of the fluid is systematically analyzed and illustrated in Figures 8–12. Figure 8 portrays the effect of the impermeability parameter ϕ_p on the velocity profile. As ϕ_p value decreases, the profile tends to increase. The reason behind this is the reduced resistance of fluid flow in impermeable media. In the impermeable case, there will be no resistance against the fluid flow, hence increasing its speed of movement. An increase in ϕ_p value will further exaggerate this effect, resulting in a decrease in the velocity. Figure.9 shows how the magnetohydrodynamic parameter affects the velocity profile. With decrease in the value of M_p, there is a tendency for the profile to boost. This is as a result of the effect of the magnetic field on the fluid flow through the exertion of the Lorentz force that hinders the flow of the fluid and hence increasing its velocity. The magnetic field has the effect of offering resistance to the flow of charged particles in the fluid, hence reducing the velocity profile. Behavior of curvature parameter γ towards the velocity profile is shown in Figure.10. It is observed that velocity and thickness of the boundary layer decrease near the surface of the cylinder but opposite effect is seen when moving away from the surface of the cylinder. This happens because of resistance of the viscous force near the surface of the cylinder, which is much more than the resistance in the absence of the surface. As the value of η varies from 0 to 1.1, the behavior of velocity profile is reversed; i.e., as curvature parameter γ increases, the radius of the cylinder decreases; hence, there is less resistance for the fluid flow. A feature of mixed convection parameter λ on velocity profiles is shown in Figure.11. It can be seen that with the increase in λ values of velocity and momentum boundary layers decrease. The mixed convection parameter is defined as the ratio of buoyancy to inertial forces. It should be noted that $\lambda = 0$ and $\lambda \neq 0$ represent the absence and presence of mixed convection parameter, correspondingly. Moreover, $\lambda > 0$ implies that the heat transfer occurs from the cylinder surface to the fluid; that is, the surface of cylinder is cooled while the fluid is heated. The increment

in value of mixed convection parameter λ causes increase in $(T_c - T_0)$ and buoyancy forces. Figure.12 describes how the velocity profile varies with respect to the viscoelastic parameter β. When β increases, not only the velocity but also the thickness of the momentum boundary layer increases. This is consistent with the expression of β from Eq.(22), where β increases with a reduction in viscosity. Therefore, the fluid flows easily and hence there is an increment in the velocity profile.

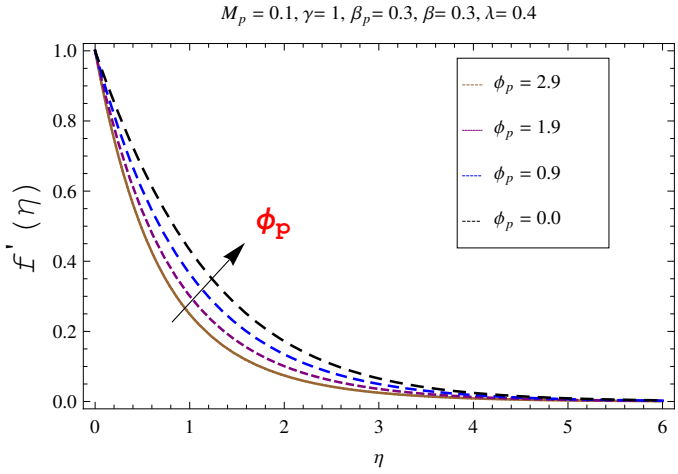


Figure 8: The impact of the porosity parameter ϕ_p on the velocity profile.

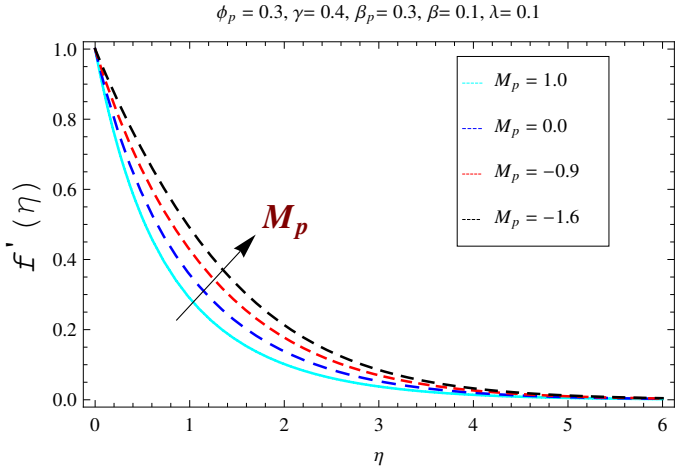


Figure 9: The impact of MHD on velocity profile.

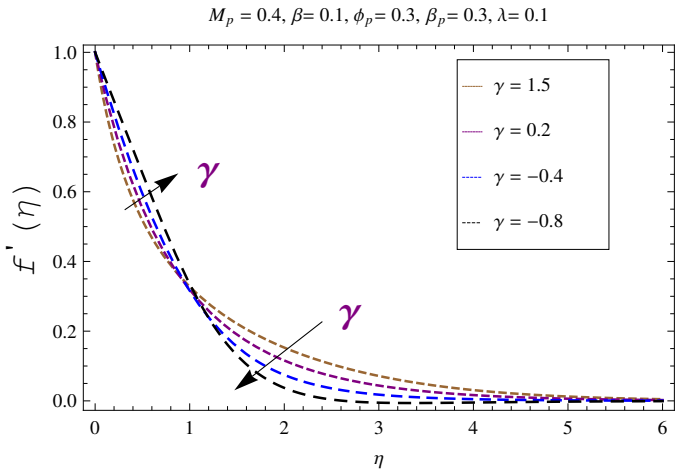


Figure 10: The impact of curvature parameter on velocity profile.

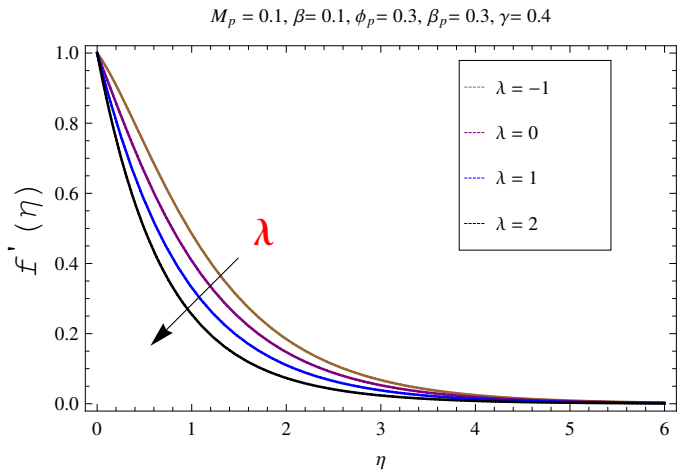


Figure 11: The impact of λ on the velocity profile.

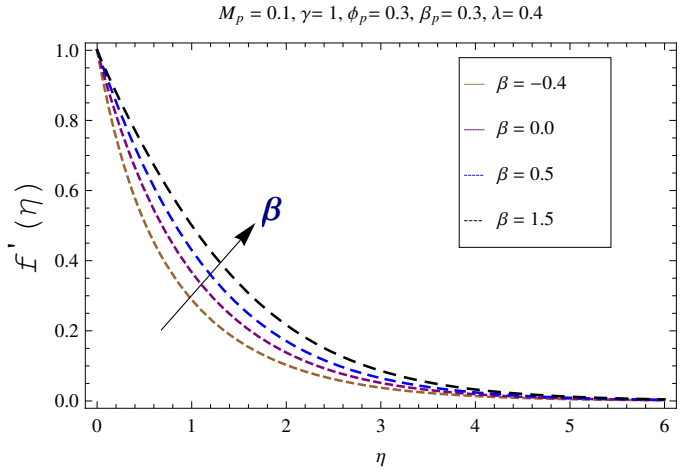


Figure 12: The impact of viscoelastic parameter β on the velocity profile.

Temperature Profiles

The effect of different parameters on the temperature distribution is examined and depicted in Figures 13 and 14. Figure.13 shows the influence of γ on the temperature distribution. It is evident from the graph that both the temperature and the thickness of the thermal boundary layer reduce near the cylinder, but show a different trend farther from the cylinder. Since η starts from zero and goes up to approximately 1.2, it can be seen that the temperature distribution graph varies in the opposite manner. As the value of the curvature parameter γ increases, the heat transfer from the cylinder to the fluid increases; hence, there is a reduction in the temperature distribution near the cylinder. Variation in the temperature distribution for variable thermal conductivity parameter ϵ is illustrated in Figure.14; it can be seen that the temperature distribution reduces with decrease in ϵ, due to temperature-dependent thermal conductivity.

Concentration Profiles

The effect of γ on the concentration distribution studied and plotted in Figure. 15. It is evident that the mass concentration as well as the boundary layer thickness becomes smaller when approaching the cylinder surface, whereas it becomes greater when moving away from the surface. As soon as η begins with 0 and reaches to about 2 (the turning point), the reverse happens in the behavior of the concentration distribution, i.e., due to the reduction of curvature

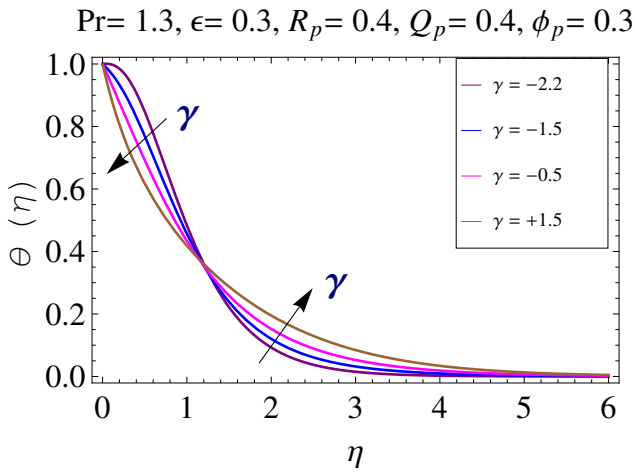


Figure 13: Influence of curvature parameter on temperature profile.

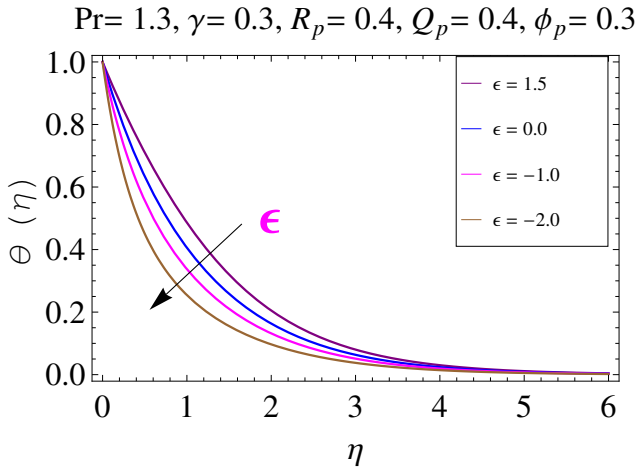


Figure 14: Influence of variable thermal conductivity parameter on the temperature profile.

parameter the rate of mass transfer from the cylinder to the fluid becomes smaller.

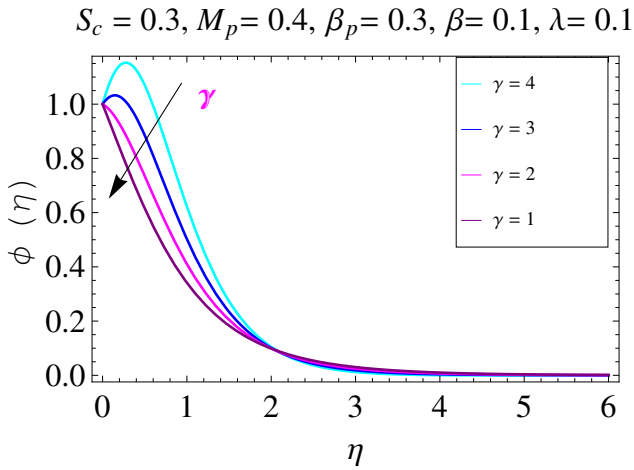


Figure 15: Influence of curvature parameter on concentration profile.

3D Profiles of Skin fraction, Nusselt and Sherwood number against different parameters

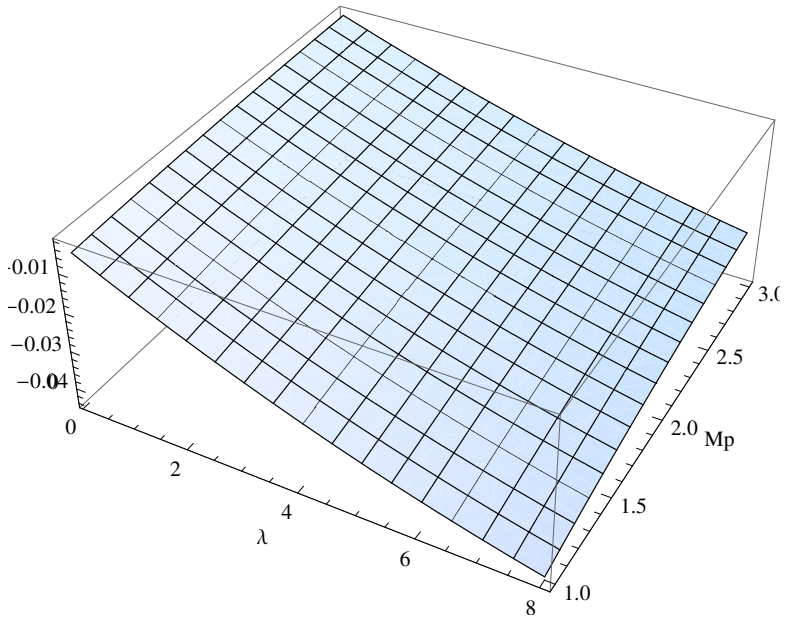


Figure 16: Profiles of $f''(0)$ against λ and different values of M_p

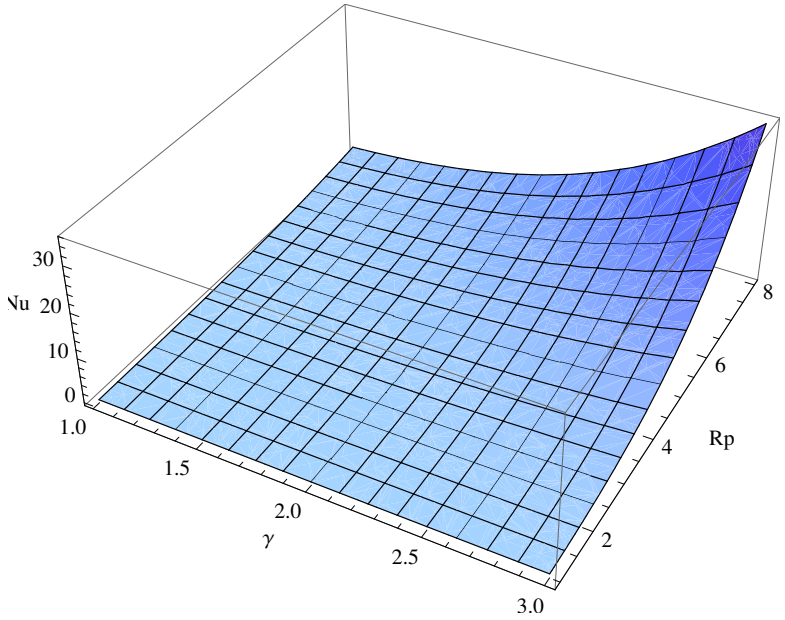


Figure 17: Profiles of $\theta'(0)$ against γ and different values of R_p

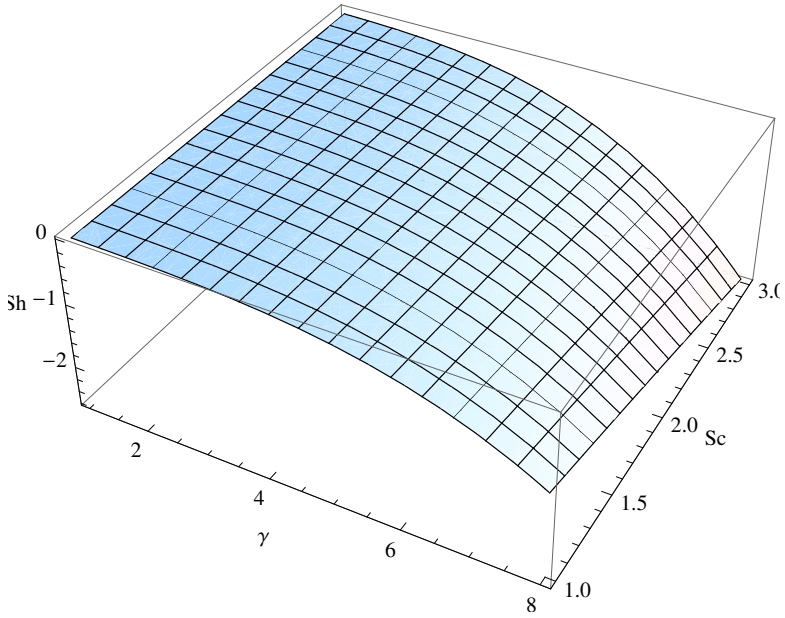


Figure 18: Profiles of $\phi'(0)$ against γ and different values of S_c

To capture the coupled variations of the flow characteristics, the results are plotted as 3D surfaces in Figures (16–18). Figure 16 depicts the three-dimensional profile for $f''(0)$ against λ and M_p. The 3D surface shows $f''(0)$ varying concurrently with λ and M_p. The entirely negative domain of $f''(0)$ indicates that the surface exerts a continuous drag force on the fluid. The surface slopes sharply downward as λ increases, showing an enhanced frictional drag. Figure 17 displays the 3D surface behavior of the Nusselt number $\theta'(0)$ as a function of γ and R_p. An upward trend in the surface topology is observed with increasing R_p, confirming that the magnitude of heat transfer enhances with higher thermal radiation parameters. Figure 18 demonstrates the 3D variation of the Sherwood number $\phi'(0)$ against γ and S_c. The surface shows a downward inclination along the S_c axis, demonstrating that the magnitude of mass transfer decreases as the Schmidt number increases.

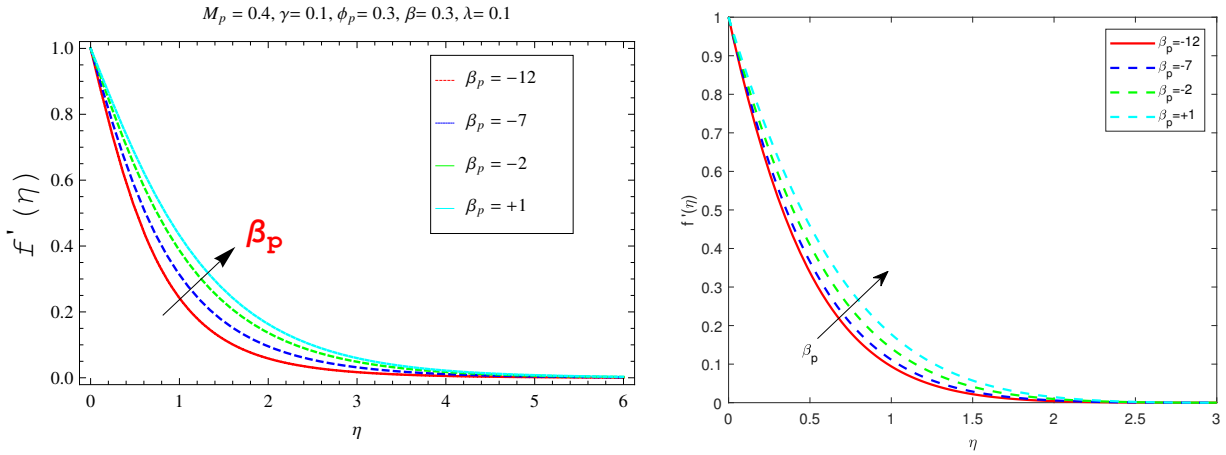
Comparison of the modeled problem with classical results To confirm the accuracy and validity of the modeled problem, the present solutions are compared with those obtained from the two employed methods as well as with the classical results. The corresponding comparisons are provided in Tables 1–2 and Figures 19–23.

Table 1: $\lambda = 0.3, \epsilon = 0.2, \gamma = 0.1, Pr = 1, \beta = 0.2, n = 2, \beta_p = 0, M_p = 0, \phi_p = 0, R_p = 0, S_c = 0$, and $Q_p = 0$.

HAM order	**HAM results of [24]**		**HAM present results**			**Numerical results**		
	$f''(0)$	$\theta'(0)$	$f''(0)$	$\theta'(0)$	$\phi'(0)$	$f''(0)$	$\theta'(0)$	$\phi'(0)$
1	-0.7971	-1.1654	-0.7971	-1.1654	-0.7111	-0.7540	-1.2217	-0.3659
5	-0.7809	-1.2559	-0.7809	-1.2559	-0.4564	-0.7540	-1.2217	-0.3659
15	-0.7762	-1.2617	-0.7762	-1.2617	-0.3657	-0.7540	-1.2217	-0.3659

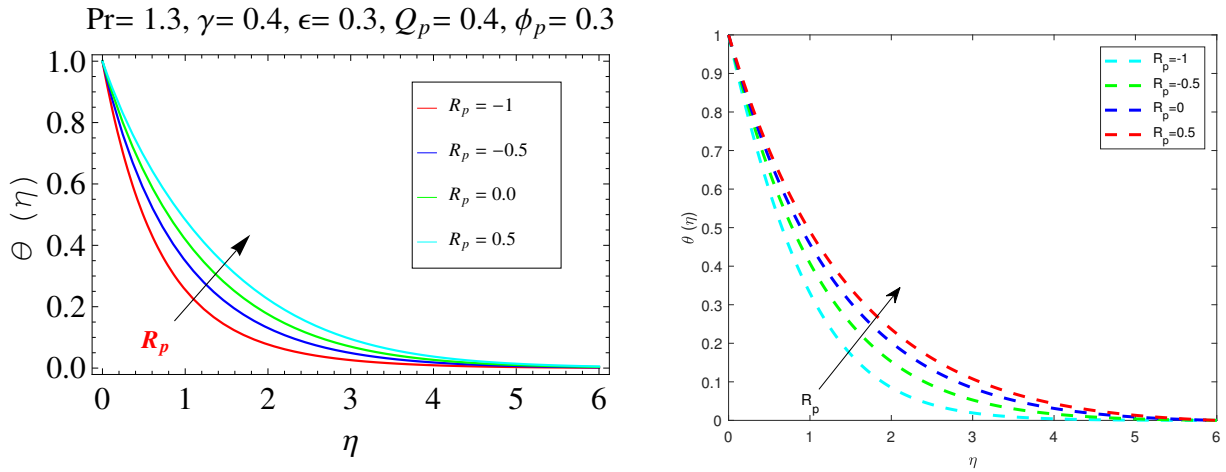
Table 2: $\lambda = 0.3, \epsilon = 0.2, Pr = 1, \beta = 0.2, n = 2, \beta_p = 0.3, M_p = 0.1, \phi_p = 0.3, R_p = 1.3, S_c = 0.4$, and $Q_p = 0.4$.

Parameter	Present series solution			Present numerical solution		
	$f''(0)$	$\theta'(0)$	$\phi'(0)$	$f''(0)$	$\theta'(0)$	$\phi'(0)$
$\gamma = 0.0$	-2.4078	-0.9233	-0.3777	-2.4078	-0.9233	-0.3777
$\gamma = 1.0$	0.2847	-2.1253	-1.9132	0.2847	-2.1253	-1.9132
$\gamma = 1.5$	0.2709	-3.2712	-3.1353	0.2709	-3.2712	-3.1336
$\gamma = 2.0$	0.2178	-4.1236	-4.1007	0.2178	-4.1236	-4.1005



(a) HAM approach **(b)** bvp4c approach

Figure 19: Influence of β_p on velocity profile.

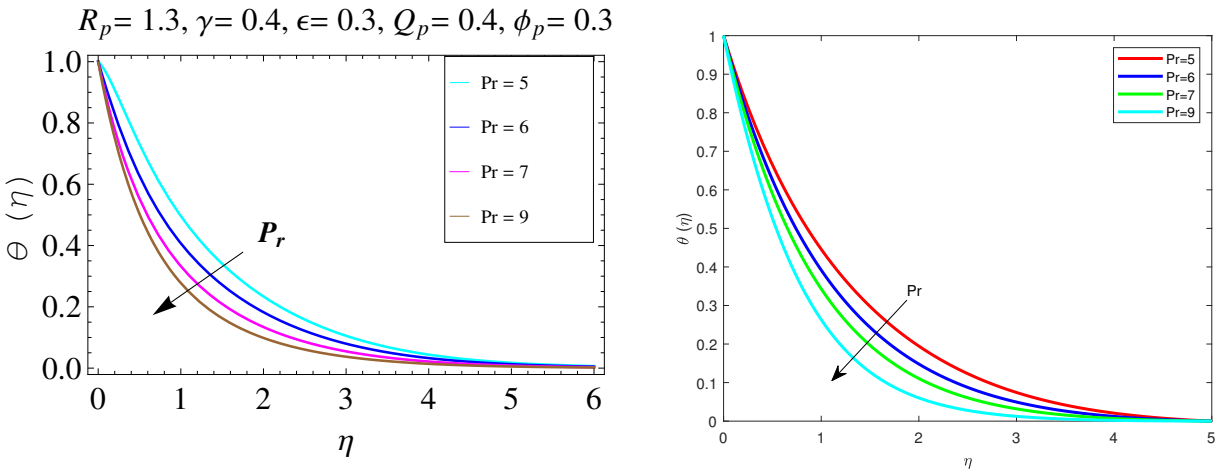


(a) HAM approach **(b)** bvp4c approach

Figure 20: Influence of R_p on temperature profile.

Figures 19 ((a) & (b)) are plotted for both HAM and bvp4c techniques to demonstrate the impact of β_p, which is representative of the Maxwell fluid, symbolizing the viscoelastic nature of the fluid on velocity profiles. There is an increase in the velocity as well as the associated momentum boundary layer thickness with an increase in β_p. The results yielded by the two methods match perfectly, which verifies the precision of the solution. Figures 20 ((a) & (b)) depict the impact of radiation parameter R_p on the temperature profile, which indicates an

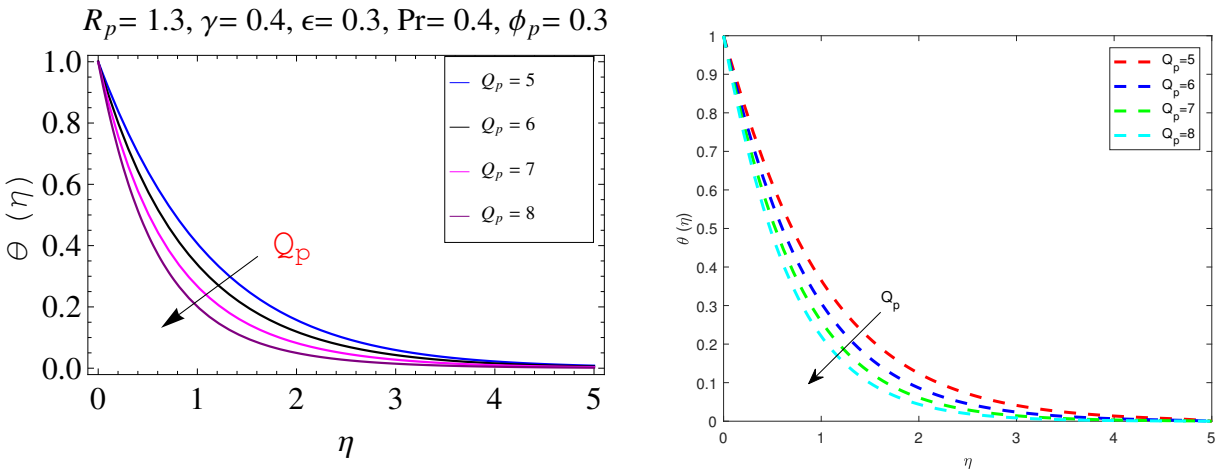
increasing trend with the increase in the radiation parameter. This phenomenon happens due to the fact that there is increased heat transfer through the radiative mechanism in the fluid. An increase in the radiation parameter means that more thermal energy will be absorbed by the fluid from the radiation sources, which leads to a sharp increase in the temperature profile.



(a) HAM approach **(b)** bvp4c approach

Figure 21: Influence of Pr on temperature profile.

Influence of Pr on temperature profile is illustrated in Figure.21 ((a) & (b)). It is noted that temperature and thickness of thermal boundary layer decreases with an increase in Pr. As the value of Prandtl number increases, thermal diffusivity decreases, causing the temperature profile to decrease. Prandtl number controls the ratio of momentum boundary layer to the thermal boundary layer. In case of large values of Prandtl number, heat diffusion happens at a slow rate, thus making the thermal boundary layer thin as compared to the lower values of Prandtl number. In case of small values of Prandtl number, heat diffusion happens faster due to thick thermal boundary layer than that in case of large Prandtl number.

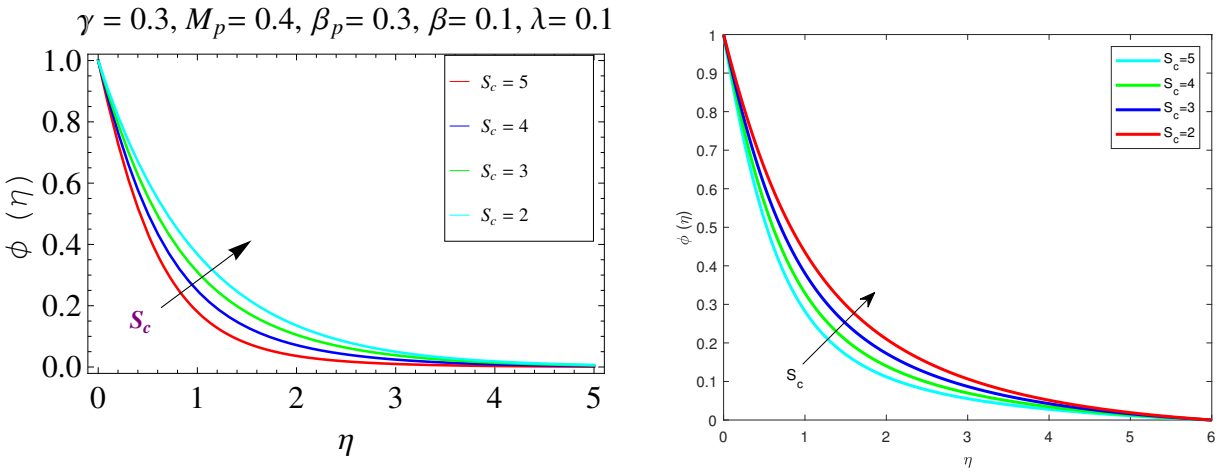


(a) HAM approach **(b)** bvp4c approach

Figure 22: Influence of Q_p on temperature profile.

Figure.22 ((a) & (b)) clearly compares the influence of the heat generation parameter Q_p on the temperature distribution, where the temperature profile is seen to increase with the increase in the value of the heat generation parameter. This is attributed to the fact that heat generation inside the fluid results in thermal energy, thus decreasing temperature. With the increase in the

heat generation parameter Q_p, less amount of heat is generated inside the fluid, thus leading to a thicker thermal boundary layer and higher temperature distribution. The heat generated further makes it easier for the fluid to conserve heat energy, thus making the temperature low.



(a) HAM approach **(b)** bvp4c approach

Figure 23: Influence of S_c on concentration profile.

Fig.23 ((a) & (b)) compares the variation of S_c for different Schmidt numbers. It is clear that when the Schmidt number becomes smaller, the concentration of the material in the fluid becomes larger. This inverse relation exists because of low diffusivity of the material as compared with the momentum diffusion in high Schmidt numbers. Furthermore, the Schmidt number plays an important role in controlling the concentration because of its effect on the diffusion of mass and momentum and their coupling.

All the above figures clearly indicate that the fluid velocity $f'(\eta)$, temperature $\theta(\eta)$ and concentration $\phi(\eta)$ decrease from 1 to 0 when distance from the stretching cylinder increases.

The table summarizes the key experimental insights derived from the present results, along with their corresponding engineering and practical applications.

Table 3: Experimental insights and practical implications

Key Insight	**Physical Interpretation (Based on Present Results)**	**Engineering & Practical Applications**
Viscoelastic fluid Enhances Heat and Mass Transfer Rate	For identical values of M_p, R_p, Pr, and Sc, the model exhibits consistent trends in the Nusselt number, skin-friction coefficient, and Sherwood number (Table 2).	In biomedical engineering, the model is relevant to magnetic therapy applications, such as drug delivery and magnetothermal treatments, where coupled mass and heat transport play a critical role.
Magnetic Field Controls Thermal and Flow Behavior	Increasing the magnetic parameter (M_p) suppresses the velocity field while increasing the temperature distribution due to the Lorentz force. Heat transfer rate is moderately affected but thermal boundary layer thickens.	Applicable in MHD pumps, electromagnetic flow control, nuclear reactor cooling, metallurgical processing, and magnetic drug-targeting systems.
Impermeable Surface Modifies Near-Wall Shear Behavior	Impermeable parameter ϕ_p on the velocity profile. The impermeable structure releases the movement of the fluid, creating less frictional resistance,which goes fast the velocity of the flow through the medium. If increases the ϕ_p, the more pronounced this effect becomes, leading to a significant reduction in velocity.	Useful in potential-flow analysis over aircraft wings and comparative studies of impermeable and porous surfaces.
Radiation Parameter Intensifies Thermal Field	A higher radiation parameter (R_p) increases the temperature field owing to enhanced radiative heat absorption.	Important for solar thermal collectors, combustion chambers, high-temperature manufacturing, and aerospace thermal shielding.
Higher Prandtl Number Reduces Thermal Diffusion	Increasing the Prandtl number (Pr) decreases thermal diffusivity and reduces the thermal boundary-layer thickness.	Relevant to polymer processing, oil-based cooling fluids, heat exchangers, and thermal insulation systems.
Analytical–Numerical Agreement Confirms Model Robustness	Excellent agreement between the HAM and `bvp4c` solutions validates the mathematical model and confirms its computational accuracy.	Provides reliable predictive capability for industrial cylindrical systems, thermal management, and engineering design optimization.

Conclusion

This work delivers a comprehensive analysis of viscoelastic second-grade fluid flow subject to mixed convection over an impermeable stretching cylinder, simultaneously accounting for MHD, radiation, and internal heat/mass generation. The key insights and methodological advancements from this study are summarized as follows:

- To overcome the formulation challenge where the fourth-order ODE lacked a matching number of initial boundary conditions, a physically motivated asymptotic decay constraint $f''(\infty) = 0$ successfully implemented. This ensured strict index consistency and numerical closure within the bvp4c algorithm.
- Moving beyond traditional 2D parametric curves, the simultaneous impacts of the governing variables were mapped using 3D surface topologies. These 3D profiles successfully exposed global behavior, non-linear coupling interactions, and critical thresholds of the skin friction coefficient, Nusselt number, and Sherwood number.
- The reliability of the results ensured through a robust dual approach such as coupling semi-analytical (HAM) and numerical (bvp4c) methods reinforced by successful validation against established experimental and classical trends from the literature.

Ultimately, this validated model proves highly reliable for optimizing engineering applications involving coupled transport phenomena such as polymer melt processing, electronic/nuclear cooling, and MHD-based thermal systems while serving as a rigorous benchmark for future complex viscoelastic flow research.

Conflict of interest

We wish to confirm that there are no known conflicts of interest associated with this publication and there has been no significant financial support for this work that could have influenced its outcome.

Funding Declaration

The authors declare that no financial support, grants, or other funding were received for the research, authorship, and/or publication of this article.

Declaration

Ethics, Consent to Participate, and Consent to Publish declaration: not applicable.

Data Availability

All data generated or analysed during this study are included in this published article.

References

Andersson, H. I., & Kumaran, V. (2006). On sheet-driven motion of power-law fluids. International Journal of Non-Linear Mechanics, 41(10), 1228-1234. doi:10.1016/j.ijnonlinmec.2006.12.006

Vajravelu, K., Prasad, K. V., & Rao, N. P. (2011). Diffusion of a chemically reactive species of a power-law fluid past a stretching surface. Computers & Mathematics with Applications, 62(1), 93-108. doi:10.1016/j.camwa.2011.04.055

Patil, P. M., Roy, S., & Pop, I. (2012). Unsteady effects on mixed convection boundary layer flow from a permeable slender cylinder due to non-linearly power law stretching. Computers & fluids, 56, 17-23. doi:10.1016/j.compfluid.2011.11.008

Lok, Y. Y., Merkin, J. H., & Pop, I. (2012). Mixed convection flow near the axisymmetric stagnation point on a stretching or shrinking cylinder. International journal of thermal sciences, 59, 186-194. doi:10.1016/j.ijthermalsci.2012.04.008

Das, K. (2012). Slip effects on MHD mixed convection stagnation point flow of a micropolar fluid towards a shrinking vertical sheet. Computers & Mathematics with Applications, 63(1), 255-267. doi:10.1016/j.camwa.2011.11.018

Liao, S. (2012). Homotopy analysis method in nonlinear differential equations (Vol. 153). Beijing: Higher education press. doi:10.1007/978-3-642-25132-0

Nadeem, S., Rehman, A., Lee, C., & Lee, J. (2012). Boundary layer flow of second grade fluid in a cylinder with heat transfer. Mathematical Problems in Engineering, 2012(1), 640289. doi:10.1155/2012/640289

Vajravelu, K., Prasad, K. V., & Santhi, S. R. (2012). Axisymmetric magneto-hydrodynamic (MHD) flow and heat transfer at a non-isothermal stretching cylinder. Applied Mathematics and computation, 219(8), 3993-4005. doi:10.1016/j.amc.2012.10.034

Moradi, A., Ahmadikia, H., Hayat, T., & Alsaedi, A. (2013). On mixed convection–radiation interaction about an inclined plate through a porous medium. International Journal of Thermal Sciences, 64, 129-136. doi:10.1016/j.ijthermalsci.2012.08.014

Hayat, T., Awais, M., & Asghar, S. (2013). Radiative effects in a three-dimensional flow of MHD Eyring-Powell fluid. Journal of the Egyptian Mathematical Society, 21(3), 379-384. doi:10.1016/j.joems.2013.02.009

Ramzan, M., Farooq, M., Alsaedi, A., & Hayat, T. (2013). MHD three-dimensional flow of couple stress fluid with Newtonian heating. The European Physical Journal Plus, 128, 1-15. doi:10.1140/epjp/i2013-13049-5

Turkyilmazoglu, M., & Pop, I. (2013). Exact analytical solutions for the flow and heat transfer near the stagnation point on a stretching/shrinking sheet in a Jeffrey fluid. International Journal of Heat and Mass Transfer, 57(1), 82-88. doi:10.1016/j.ijheatmasstransfer.2012.10.006

Shehzad, S. A., Alsaedi, A., & Hayat, T. (2013). Hydromagnetic steady flow of Maxwell fluid over a bidirectional stretching surface with prescribed surface temperature and prescribed surface heat flux. Plos One, 8(7), e68139. doi:10.1371/journal.pone.0068139

Hayat, T., Shafiq, A., Alsaedi, A., & Awais, M. (2013). MHD axisymmetric flow of third grade fluid between stretching sheets with heat transfer. Computers & Fluids, 86, 103-108. doi:10.1016/j.compfluid.2013.07.003

Abd El-Aziz, M. (2013). Mixed convection flow of a micropolar fluid from an unsteady stretching surface with viscous dissipation. Journal of the Egyptian Mathematical Society, 21(3), 385-394. doi:10.1016/j.joems.2013.02.010

Mukhopadhyay, S., De, P. R., Bhattacharyya, K., & Layek, G. C. (2013). Casson fluid flow over an unsteady stretching surface. Ain Shams Engineering Journal, 4(4), 933-938. doi:10.1016/j.asej.2013.04.004

Turkyilmazoglu, M. (2013). The analytical solution of mixed convection heat transfer and fluid flow of a MHD viscoelastic fluid over a permeable stretching surface. International Journal of Mechanical Sciences, 77, 263-268. doi:10.1016/j.ijmecsci.2013.10.011

Vajravelu, K., Prasad, K. V., & Ng, C. O. (2013). Unsteady convective boundary layer flow of a viscous fluid at a vertical surface with variable fluid properties. Nonlinear Analysis: Real World Applications, 14(1), 455-464. doi:10.1016/j.nonrwa.2012.07.008

Rashidi, M. M., Rajvanshi, S. C., Kavyani, N., Keimanesh, M., Pop, I., & Saini, B. S. (2014). Investigation of heat transfer in a porous annulus with pulsating pressure gradient by homotopy analysis method. Arabian Journal for Science and Engineering, 39, 5113-5128. doi:10.1007/s13369-014-1140-5

Hayat, T., Farooq, M., & Alsaedi, A. (2014). Melting heat transfer in the stagnation-point flow of Maxwell fluid with double-diffusive convection. International Journal of Numerical Methods for Heat & Fluid Flow, 24(3), 760-774. doi:10.1108/HFF-09-2012-0219

Mukhopadhyay, S., & Mandal, I. C. (2014). Boundary layer flow and heat transfer of a Casson fluid past a symmetric porous wedge with surface heat flux. Chinese Physics B, 23(4), 044702. doi:10.1088/1674-1056/23/4/044702

Hsiao, K. L. (2014). Conjugate heat transfer for mixed convection and Maxwell fluid on a stagnation point. Arabian journal for science and engineering, 39(6), 4325-4332. doi:10.1007/s13369-014-1065-z

Dalir, N. (2014). Numerical study of entropy generation for forced convection flow and heat transfer of a Jeffrey fluid over a stretching sheet. Alexandria Engineering Journal, 53(4), 769-778. doi:10.1016/j.aej.2014.08.005

Hayat, T., Anwar, M. S., Farooq, M., & Alsaedi, A. (2015). Mixed convection flow of viscoelastic fluid by a stretching cylinder with heat transfer. Plos one, 10(3), e0118815. doi:10.1371/journal.pone.0118815

Shah, S., Rafiq, N., Abdullah, F. A., Atif, S. M., & Abbas, M. (2022). Slip and radiative effects on MHD Maxwell nanofluid with non-Fourier and non-Fick laws in a porous medium. Case Studies in Thermal Engineering, 30, 101779. doi:10.1016/j.csite.2022.101779

Raj, U., Sagadevan, P., & Alessa, N. (2024). Effect of heat generation on MHD Maxwell fluid flow on a stretching cylinder embedded in a porous medium along with impact of radiation. Journal of King Saud University-Science, 36(11), 103530. doi:10.1016/j.jksus.2024.103530

Khan, Z. H., Khan, W. A., Ibrahim, S. M., Swain, K., & Huang, Z. (2024). Impact of multiple slips and thermal radiation on heat and mass transfer in MHD Maxwell hybrid nanofluid flow over porous stretching sheet. Case Studies in Thermal Engineering, 61, 104906. doi:10.1016/j.csite.2024.104906

Jakhar, A., Sukariya, V. K., Kumar, S., Kumar, A., & Anurag. (2024). Study of MHD Williamson fluid flow over a stretched cylinder with Hall, thermal dynamics, and chemical reactions effects. Journal of Thermal Analysis and Calorimetry, 1-18. doi:10.1007/s10973-024-13851-9

Olkha, A., Kumar, M., Choudhary, R., & Meena, S. K. (2025). Second grade slip flow over a non-linearly stretching surface with radiation effects and variable fluid properties under convective boundary condition. Mathematics in Engineering, Science & Aerospace (MESA), 16(1).

Sadeghy, K., & Sharifi, M. (2004). Local similarity solution for the flow of a "second-grade" viscoelastic fluid above a moving plate. International Journal of Non-Linear Mechanics, 39(8), 1265-1273. doi:10.1016/j.ijnonlinmec.2003.08.005

Nomenclature

α_1	second grade material parameter
β	Viscoelastic parameter
β_p	Deborah number
β_T	Coefficient of volumetric thermal expansion
ϵ	Scalar parameter
γ	Curvature parameter
λ	Mixed convection parameter
∇C	Characteristics concentration
∇T	Characteristics temperature
ϕ_p	Impermeable medium parameter
ρ	Density
σ	Stefan-Boltzmann constant
τ	Cauchy stress tensor
τ_c	Wall shear stress tensor
θ	Dimensionless temperature
B_0	Magnetic parameter
C_∞	Ambient region concentration
$C_c(x)$	Concentration of the cylinder
C_f	Skin fraction coefficient
C_p	Specific heat at constant pressure
D_B	Mass diffusion
Gr_x	Local Grashof number
j_x	Mass flux
k	Mean absorption efficient
$K(T)$	Thermal conductivity
K_∞	Thermal conductivity of the ambient fluid
l	Characteristics length
M_p	Ratio of magnetic force to inertial force
n	Surface temperature exponents

Nu_x	Nusselt number
q_c	Heat flux
Q_p	Dimensional heat generation
R_p	Radiation parameter
Re_x	Local Reynolds number
S_c	Schmidt number
Sh_x	Sherwood number
T_∞	Ambient fluid temperature
$T_c(x)$	Temperature of the cylinder surface
u, v	Velocity components
u_0	Reference velocity
$u_c(x)$	Stretching velocity
v	kinematics viscosity
Pr	Prandtl number